

LETTER • OPEN ACCESS

Mitigating ozone damage to ecosystem productivity through sectoral and regional emission controls: a case study in the Yangtze River Delta, China

To cite this article: Yadong Lei *et al* 2022 *Environ. Res. Lett.* **17** 065008

View the [article online](#) for updates and enhancements.

You may also like

- [National- to port-level inventories of shipping emissions in China](#)
Mingliang Fu, Huan Liu, Xinxin Jin et al.
- [Changes in the frequency and return level of high ozone pollution events over the eastern United States following emission controls](#)
H E Rieder, A M Fiore, L M Polvani et al.
- [Global and regional trends in particulate air pollution and attributable health burden over the past 50 years](#)
E W Butt, S T Turnock, R Rigby et al.

ENVIRONMENTAL RESEARCH
LETTERS

LETTER

OPEN ACCESS

RECEIVED
10 March 2022REVISED
29 April 2022ACCEPTED FOR PUBLICATION
16 May 2022PUBLISHED
27 May 2022

Original content from
this work may be used
under the terms of the
[Creative Commons
Attribution 4.0 licence](#).

Any further distribution
of this work must
maintain attribution to
the author(s) and the title
of the work, journal
citation and DOI.

Mitigating ozone damage to ecosystem productivity through
sectoral and regional emission controls: a case study in the
Yangtze River Delta, ChinaYadong Lei¹, Xu Yue^{2,*} , Zhili Wang¹ , Hong Liao², Lin Zhang³ , Chenguang Tian⁴, Hao Zhou⁴,
Junting Zhong¹, Lifeng Guo¹, Huizheng Che¹ and Xiaoye Zhang¹

¹ State Key Laboratory of Severe Weather and Key Laboratory of Atmospheric Chemistry of CMA, Chinese Academy of Meteorological Sciences, Beijing 100081, People's Republic of China

² Jiangsu Key Laboratory of Atmospheric Environment Monitoring and Pollution Control, Jiangsu Collaborative Innovation Center of Atmospheric Environment and Equipment Technology, School of Environmental Science and Engineering, Nanjing University of Information Science and Technology, Nanjing 210044, People's Republic of China

³ Laboratory for Climate and Ocean-Atmosphere Studies, Department of Atmospheric and Oceanic Sciences, School of Physics, Peking University, Beijing 100871, People's Republic of China

⁴ Climate Change Research Center, Institute of Atmospheric Physics, Chinese Academy of Sciences, Beijing 100029, People's Republic of China

* Author to whom any correspondence should be addressed.

E-mail: yuxu@nuist.edu.cn

Keywords: ozone, gross primary productivity, sectoral emissions, mitigation, YIBs model

Supplementary material for this article is available [online](#)

Abstract

The land ecosystems of China are estimated to provide an important sink for the increased atmospheric carbon dioxide (CO₂), but are undermined by severe ozone (O₃) pollution. Mitigation of O₃ damage to ecosystems remains a challenge considering that O₃ precursors are emitted from a wide range of anthropogenic sectors and O₃ formations are also affected by regional transport. Here, we combine chemical transport and dynamic vegetation models to quantify the benefits of sectoral and regional emission controls for the recovery of gross primary productivity (GPP) in the Yangtze River Delta (YRD). For sectoral emission controls, the largest mitigation of O₃ damage to GPP in YRD by 3.1 ± 0.4 and 2.2 ± 0.2 Gg[C] d⁻¹ with 50% reductions in the emissions from industry and transportation sectors, respectively. For regional emission controls, reducing 50% anthropogenic emissions outside YRD can mitigate GPP losses by 18.6 ± 3.5 Gg[C] d⁻¹, larger than the recovery of 10.1 ± 1.6 Gg[C] d⁻¹ by the 50% reductions of anthropogenic emissions within YRD. Moreover, summer months, especially July are the best period for GPP recovery from anthropogenic emission controls. Our results highlight the importance of sectoral and regional emission controls to mitigate O₃ damage to ecosystem productivities in YRD.

1. Introduction

Ozone (O₃) and haze episodes are two emerging and connected challenges in China (Li *et al* 2019, Ma *et al* 2021, Qu *et al* 2021, Zhao *et al* 2022). Since 2013, stringent air pollution control named 'Clean Air Actions' has been implemented by Chinese government to solve the air quality problem. Consequently, concentrations of particulate matter decreased substantially ever since (Fu *et al* 2019, Zhang *et al* 2019, He *et al* 2021). However, O₃ pollution is getting worse (Liu and Wang 2020, Lu *et al* 2020,

Dang *et al* 2021), especially in Yangtze River Delta (YRD) where the ratio of O₃-dominated episodes increased from 13.9% in 2013 to 50.4% in 2017 (www.cnemc.cn/jcbg/zghjzkgb/). As a secondary gas pollutant, O₃ is produced by chemical reactions of nitrogen oxides (NO_x) and volatile organic compounds (VOCs) in the presence of sunlight (Atkinson 2000, Chen and Brune 2012). In China, O₃ precursors such as NO_x and VOCs are mainly emitted by anthropogenic sources, including industry, transportation, and power sectors (Lu *et al* 2019, Li *et al* 2020). Meanwhile, surface O₃ is likely to reach high levels on

hot and sunny days due to accelerated photochemical rates and reduced plant stomatal uptake (Gong and Liao 2019, Lin *et al* 2020, Lei *et al* 2022).

High O₃ concentrations near surface can not only threaten human health (Chen *et al* 2012, Lu *et al* 2020), but also reduce terrestrial ecosystem productivity (Yue *et al* 2017, Agathokleous *et al* 2020, Unger *et al* 2020, Lei *et al* 2021). Open-top chambers and free-air experiments revealed visible O₃ injuries on numerous plant species, including trees, shrubs, and herbs (Wan *et al* 2014, Feng *et al* 2015). Based on these measurements, some O₃ vegetation damage schemes were developed, for example Sitch *et al* (2007) and Lombardozi *et al* (2015), to predict reductions in photosynthesis using O₃ stomatal uptake and empirical damaging sensitivities. Numerical models implementing these schemes showed that O₃ causes strong damages to ecosystem productivity from regional to global scales (Zhou *et al* 2018, Unger *et al* 2020).

Ecosystem is an important carbon sink in China. Every year, terrestrial ecosystem uptakes ~10% of the total anthropogenic carbon emissions in China (Piao *et al* 2009, Fang *et al* 2018). However, the land sink capacity in China is threatened by the worsening O₃ pollution that induces losses of ~15% in ecosystem productivity (Yue *et al* 2017, Unger *et al* 2020). Therefore, how to mitigate O₃ damages on land ecosystem productivity is an urgent question. Here, we combine chemical transport and dynamic vegetation models to examine how much carbon loss can be avoided through sectoral and regional emission controls of O₃ precursors. We focus specifically on the land ecosystems in YRD, where vegetation cover is high and O₃ level was increasing fast in recent years. Emission controls include stringent 50% reductions in anthropogenic emissions from five sectors and different regions, a decreasing ratio likely achieved by the 2060s with the national carbon neutrality target (Tong *et al* 2020, Lamboll *et al* 2021, He *et al* 2022). Surface O₃ is predicted by the chemical transport model under different emission controls, and is then used to influence carbon cycle in the vegetation model.

2. Methods and materials

2.1. The GEOS-Chem chemical transport model

GEOS-Chem is a widely used global 3D chemical transport model for simulating concentrations of gas-phase pollutants and aerosols with a detailed HO_x–NO_x–VOC–O₃–halogen–aerosol chemistry mechanism (Kim *et al* 2015a, Lee *et al* 2017, Lu *et al* 2019, Porter and Heald 2019, Gong *et al* 2021). This model uses Fast-JX scheme to compute photolysis rates (Bian and Prather 2002). Biogenic VOC (BVOC) emissions are computed based on the Model of Emissions of Gases and Aerosols from Nature

(MEGAN v2.1) (Guenther *et al* 2012). The dry deposition for gases is computed based on the resistance-in-series scheme (Wesely 1989). The global anthropogenic emission inventory is obtained from Community Emissions Data System (Hoesly *et al* 2018). Anthropogenic emissions in China are computed based on Multiresolution Emission Inventory (MEIC), which estimates SO₂, NO_x, CO, NMVOC, NH₃, PM₁₀, PM_{2.5}, BC, OC, and CO₂ emissions from five source sectors including agriculture (AGR), industry (IND), power (POW), residential (RES), and transportation (TRA) (Zheng *et al* 2018). Notably, agriculture source sector only includes NH₃ emissions. Total anthropogenic emissions from each sector in YRD are summarized in table S1 (available online at stacks.iop.org/ERL/17/065008/mmedia). In this study, nested GEOS-Chem version 12.0.0 with resolution of 0.5° × 0.625° is driven by the Modern-Era Retrospective analysis for Research and Applications, version 2 (MERRA2) meteorological fields to predict the changes of tropospheric O₃ under different anthropogenic emission controls.

2.2. The Yale Interactive terrestrial Biosphere (YIBs) vegetation model

The YIBs model is a process-based vegetation model designed to simulate global carbon cycle with dynamical prediction of leaf area index (LAI) and tree height (Yue and Unger 2015). Leaf-level photosynthesis is computed using Farquhar *et al* (1980) scheme. The leaf photosynthesis is further upscaled to canopy level by separating the responses of sunlit and shaded leaves to diffuse and direct radiation (Spitters 1986). Calculations of LAI and carbon allocation follow the Joint UK Land Environment Simulator (JULES) model (Clark *et al* 2011). The Moderate Resolution Imaging Spectroradiometer (MODIS) land types and cover fractions are aggregated into eight plant functional types (figure S1), including evergreen needleleaf forest, deciduous broadleaf forest, evergreen broadleaf forest, shrubland, C₃/C₄ grasses, and C₃/C₄ crops to calculate carbon uptake in the YRD. The YIBs model applies Kim *et al* (2015b) scheme to build phenology. For crops, the plant date and harvest date are fixed based on observations. For other plant functional types, leaf phenology is generally controlled by temperature, water availability, and photoperiod. The YIBs model has been comprehensively validated against site-level observations and satellite retrievals (Yue *et al* 2015, 2017, Yue and Unger 2018). Since 2020, the YIBs model has joined the multi-model ensemble project ‘Trends in the land carbon cycle (TRENDY)’ to estimate global carbon budget (Friedlingstein *et al* 2020). In this study, the YIBs model is driven by the same meteorological fields (MERRA2) as GEOS-Chem with a higher resolution of 0.25° × 0.3125°.

The semi-mechanistic O₃ damage scheme is coupled into YIBs to quantify the carbon losses by

surface O_3 (Sitch *et al* 2007, Lei *et al* 2020, Unger *et al* 2020). The O_3 -induced photosynthesis loss (A' , $\mu\text{mol m}^{-3}$) is calculated by multiplying the O_3 damage factor (α) to the original leaf photosynthesis (A , $\mu\text{mol m}^{-3}$):

$$A' = A \times \alpha. \quad (1)$$

The α is calculated based on excessive O_3 flux (EF_{O_3} , $\mu\text{mol m}^{-2}\text{s}^{-1}$) and sensitivity coefficient (β):

$$\alpha = EF_{O_3} \times \beta. \quad (2)$$

The β has two values for each vegetation type, representing low to high O_3 -damaging sensitivities. The EF_{O_3} is calculated based on stomatal O_3 flux (F_{O_3} , $\mu\text{mol m}^{-2}\text{s}^{-1}$) and O_3 damaging threshold (T_{O_3} , $\mu\text{mol m}^{-2}\text{s}^{-1}$):

$$EF_{O_3} = \max(F_{O_3} - T_{O_3}, 0). \quad (3)$$

The T_{O_3} represents the O_3 tolerance for each vegetation type. The F_{O_3} is calculated based on surface O_3 concentrations ($[O_3]$, $\mu\text{mol m}^{-3}$), aerodynamic resistance (R_a , s m^{-1}), boundary layer resistance (R_b , s m^{-1}), stomatal conductance (R_s , s m^{-1}), and the ratio of leaf resistance O_3 to leaf resistance of water vapor (k):

$$F_{O_3} = [O_3] / (R_a + R_b + k \times R_s). \quad (4)$$

The O_3 -damaging gross primary productivity (GPP) is calculated by integrating A' over all canopy layers:

$$GPP' = \int_0^{LAI} A' dL. \quad (5)$$

This scheme has been well validated against hundreds of experimental data collected globally and in China (Yue *et al* 2017, Yue and Unger 2018).

2.3. Model simulations

In this study, we conduct ten GEOS-Chem runs and 20 YIBs runs to explore the changes of O_3 -induced GPP reductions in the YRD by different anthropogenic emission control strategies (table 1). In the control run (CTRL), the GEOS-Chem model is forced with all sources of emissions. The SHUT run uses the same emissions as CTRL, except for shutting down anthropogenic emissions in China. In five sensitivity runs, the model is forced with all anthropogenic emissions but 50% emission reductions in YRD from a specific sector, including agriculture (AGR_RED50%), industry (IND_RED50%), power (POW_RED50%), residential source (RES_RED50%), or transportation (TRA_RED50%). We perform another three runs with GEOS-Chem to explore the impacts of collaborative emission reductions and regional

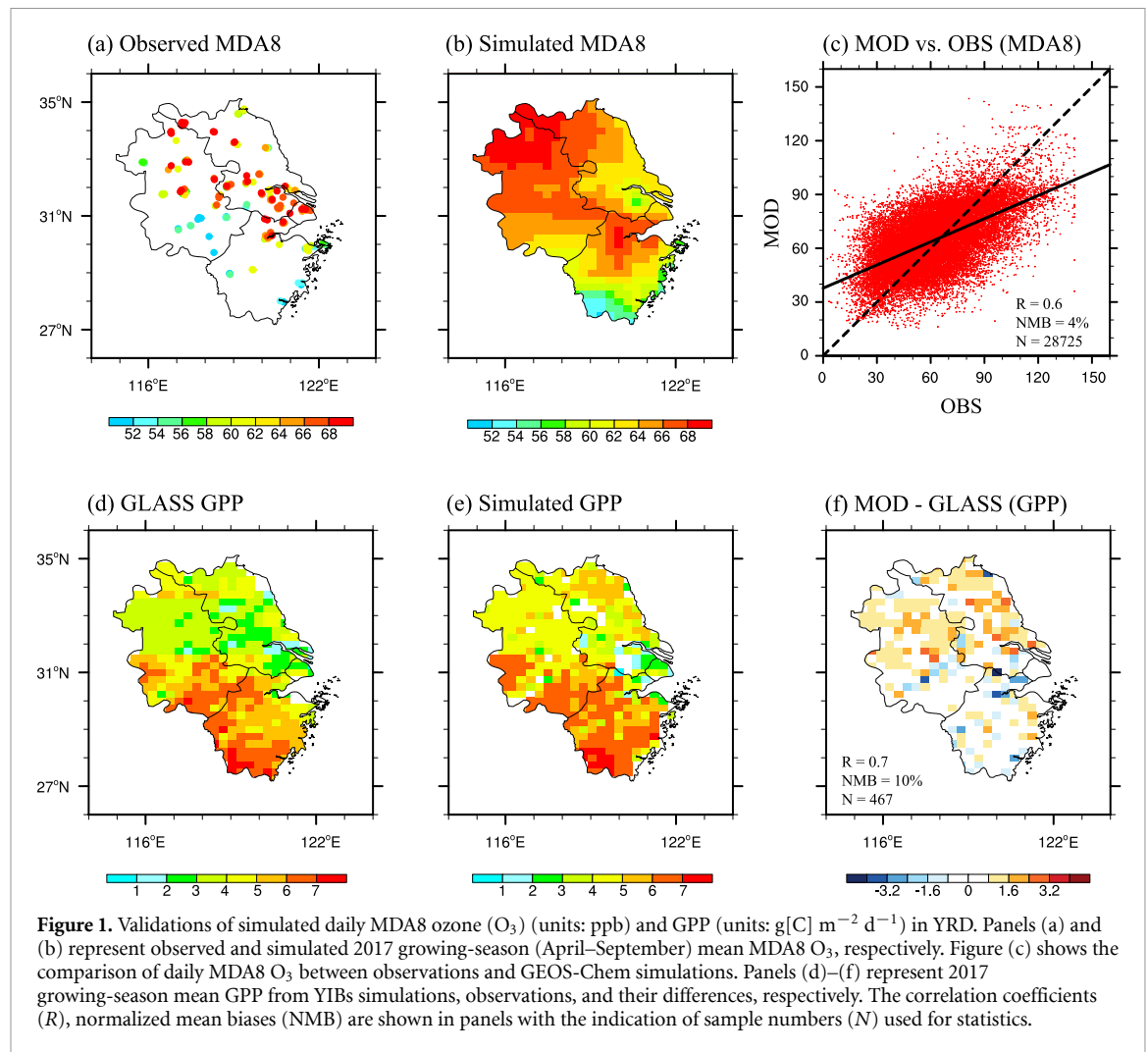
Table 1. Summary of simulations with GEOS-Chem models.

Name	Emissions
CTRL	All emissions
SHUT	Shut down anthropogenic emissions in China
AGR_RED50%	Reduce agriculture emissions alone by 50% in YRD
IND_RED50%	Reduce industry emissions alone by 50% in YRD
POW_RED50%	Reduce power emissions alone by 50% in YRD
RES_RED50%	Reduce residential emissions alone by 50% in YRD
TRA_RED50%	Reduce transportation emissions alone by 50% in YRD
YRD _{out} _RED50%	Reduce anthropogenic emissions by 50% outside YRD
YRD _{in} _RED50%	Reduce anthropogenic emissions by 50% in YRD
CHN_RED50%	Reduce anthropogenic emissions by 50% in China

transport on O_3 pollution, including 50% reductions of anthropogenic emissions outside YRD (YRD_{out}_RED50%), inside YRD (YRD_{in}_RED50%), or the whole anthropogenic emissions in China (CHN_RED50%). For above simulations, anthropogenic emissions of all pollution species are retained or perturbed with the same ratios (e.g. reduce by 50% or 100%). All runs are conducted from January to September in 2017 and the results of last 6 months are used to investigate the mitigation effects of anthropogenic emission controls on O_3 -induced GPP losses during the growing season (April–September). The simulated hourly surface O_3 concentrations from each GEOS-Chem run are used to drive the YIBs model with either high or low sensitivities, making a total of 20 YIBs runs. The derived GPP losses with low and high O_3 -damaging sensitivities are averaged for comparisons and one standard deviation of low and high O_3 -damaging sensitivities represents uncertainties of O_3 damage on GPP.

2.4. Validation data

Ground-based hourly O_3 concentrations in 2017 growing-season are collected from the observational network of the China Ministry of Ecology and Environment (MEE) (<http://datacenter.mee.gov.cn/>). With quality control, continuous measurements at 157 sites in YRD are selected to evaluate the simulated surface O_3 from GEOS-Chem. We use the daily maximum 8 h average (MDA8) O_3 as the metric in validation. Benchmark GPP are obtained from the Global Land Surface Satellite (GLASS) product generation system (Yuan *et al* 2010, Zhao *et al* 2013). The GLASS GPP agrees well with FLUXNET observations (Yu *et al* 2018) and has been widely used in the estimate of global and regional carbon budgets (Jiang *et al* 2021).



3. Results

3.1. Model validations

Simulated mean surface O_3 concentrations and GPP during the growing season in 2017 are validated using site-level measurements from MEE and benchmark GPP from GLASS (figure 1). We choose 2017 here as the regional MEIC inventory used in GEOS-Chem is only updated to 2017 (<http://meicmodel.org/>). Observed O_3 shows high values in the north and east of YRD (figure 1(a)), following the large regional emissions (figure S2). Compared to observations, the GEOS-Chem model well captures the spatiotemporal variation of surface O_3 , with a high correlation coefficient of 0.6 ($p < 0.01$) and a low normalized mean bias of 4% for 28725 statistical samples (figures 1(b) and (c)). Similarly, the YIBs model reasonably depicts the spatial distribution of GPP with an increasing gradient from the north to the south of YRD (figures 1(d) and (e)). The correlation coefficient is 0.7 ($p < 0.01$) and the normalized mean bias is only 10% for 467 statistical samples between observations and simulations (figure 1(f)). The limited biases in both the simulated O_3 and GPP consolidate our strategies in

quantifying the changes of O_3 -induced carbon losses under different emission controls using the GEOS-Chem and YIBs models.

3.2. O_3 damage to ecosystem productivity

Ecosystem productivity in YRD is threatened by the severe O_3 pollution (figure 2). In 2017, surface O_3 reduces regional GPP by $184.1 \pm 44.5 Gg[C] d^{-1}$ during the growing season in YRD (figure 2(a)), accounting for a fraction of 10% to the total GPP. Regional maximum reductions are distributed in Zhejiang province and southern Anhui province, although the high surface O_3 concentrations are predicted in the northern Anhui province and southern Jiangsu province. Such discrepancy is likely because that northern Anhui province and southern Jiangsu province is mainly covered by crops which have a higher O_3 damage critical threshold than other ecosystem types (Unger *et al* 2020). In the growing season, O_3 -induced GPP reductions reach maximums in summer (June–August) due to large GPP and high surface O_3 concentrations (figure 2(c)). With sensitivity simulation SHUT, we quantify the effects of anthropogenic emissions on

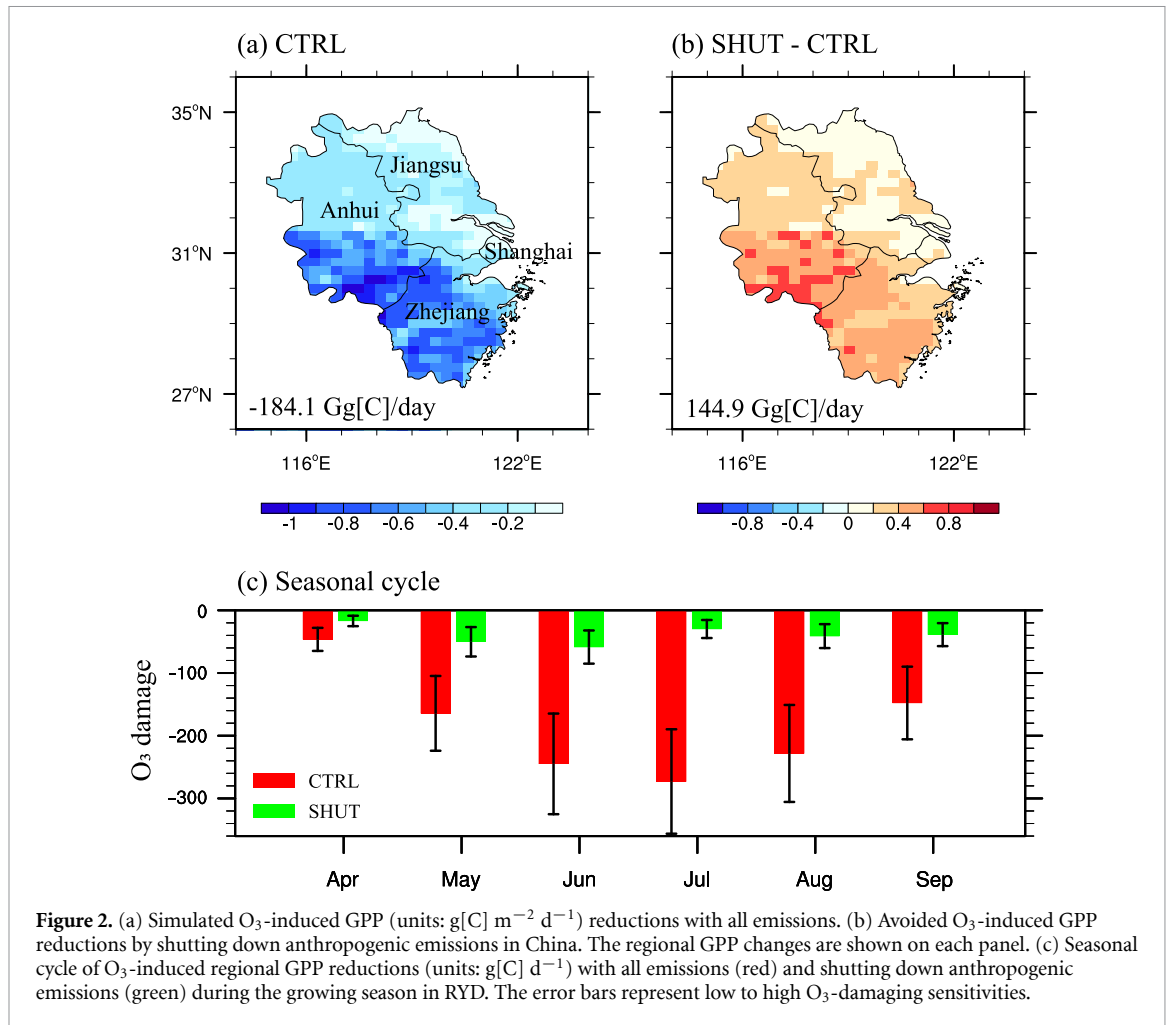


Figure 2. (a) Simulated O₃-induced GPP (units: g[C] m⁻² d⁻¹) reductions with all emissions. (b) Avoided O₃-induced GPP reductions by shutting down anthropogenic emissions in China. The regional GPP changes are shown on each panel. (c) Seasonal cycle of O₃-induced regional GPP reductions (units: g[C] d⁻¹) with all emissions (red) and shutting down anthropogenic emissions (green) during the growing season in RYD. The error bars represent low to high O₃-damaging sensitivities.

ecosystem productivity in YRD. It is found that shutting down all anthropogenic emissions in China decreases regional mean O₃ by 29.2 ppbv during the growing season in YRD (figure S3(a)). Consequently, O₃-induced GPP loss is alleviated by 144.9 ± 31.5 Gg[C] d⁻¹ in YRD (figure 2(b)). The largest benefit of GPP recovery occurs in July in response to the largest O₃ reduction by shutting down all anthropogenic emissions (figures 2(c) and S3(b)). Although anthropogenic emissions contribute only 45% to the total surface O₃, shutting down anthropogenic emissions helps mitigate 79% of total O₃-induced Δ GPP during the growing season in YRD. Therefore, exploring the effects of anthropogenic emission controls on O₃-induced Δ GPP is of great value for ecosystem health in YRD.

3.3. Changes of surface O₃ by sectoral and regional emission controls

Simulated surface O₃ in YRD is influenced by different anthropogenic emission control strategies (figure 3). For 50% anthropogenic emission reductions in industrial and transportation sectors, regional mean surface O₃ in YRD decreases by 0.6 and 0.4 ppbv during the growing season, respectively (figures 3(b) and (e)). In contrast, regional mean

surface O₃ increases by 1.0 ppbv during the growing season with 50% reductions in agriculture emissions (figure 3(a)). For this specific sector, emissions are mainly in the form of ammonia, the reduction of which does not affect O₃ precursors but decrease ammonium and PM_{2.5} concentrations (figure S4). Consequently, the reductions of aerosols reduce the uptake of HO₂ and results in more production of surface O₃ (Li et al 2019). As a comparison, reductions of anthropogenic emissions in other sectors such as power and residential have smaller impacts on surface O₃ with regional mean changes of 0.2 and 0.1 ppbv, respectively (figures 3(c) and (d)).

Compared to emission controls of a single sector, collaborative emission reductions have better effects in the mitigation of O₃ pollution. For 50% emission reductions in all sectors within YRD, regional mean surface O₃ shows a large reduction of -2.0 ppbv during the growing season (figure 3(f)), which has better mitigation effects than the sum of independent emission reductions of five sectors (figures 3(a)–(e)). This is because that there are inhomogeneous emissions for O₃ precursors, such as NO_x and VOCs from different sectors. For example, power sector accounts for 20% of total NO_x emissions but only <1% of total VOCs emissions. Thus, anthropogenic

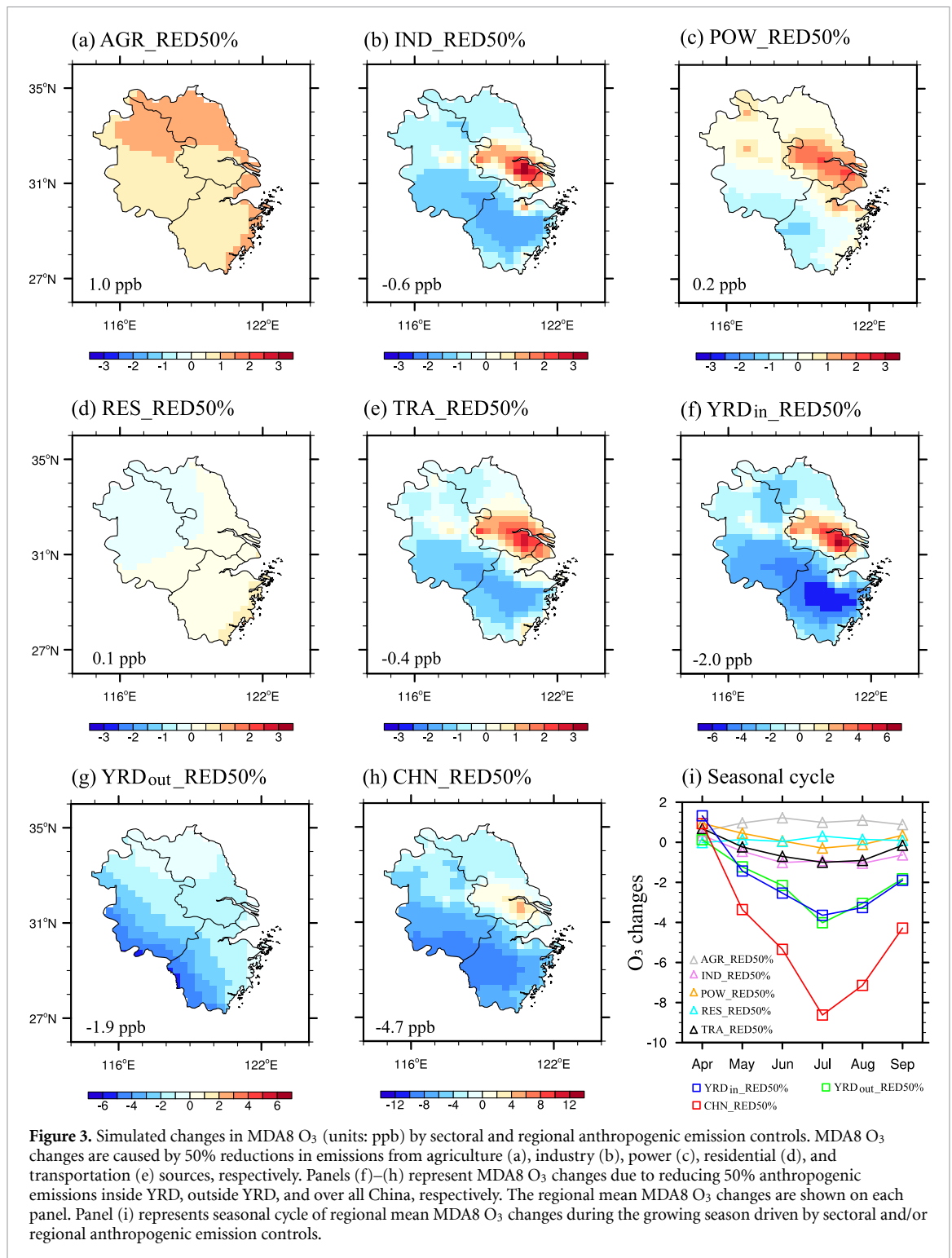


Figure 3. Simulated changes in MDA8 O₃ (units: ppb) by sectoral and regional anthropogenic emission controls. MDA8 O₃ changes are caused by 50% reductions in emissions from agriculture (a), industry (b), power (c), residential (d), and transportation (e) respectively. Panels (f)–(h) represent MDA8 O₃ changes due to reducing 50% anthropogenic emissions inside YRD, outside YRD, and over all China, respectively. The regional mean MDA8 O₃ changes are shown on each panel. Panel (i) represents seasonal cycle of regional mean MDA8 O₃ changes during the growing season driven by sectoral and/or regional anthropogenic emission controls.

emission control from power sector means only NO_x emissions reductions, which will increase surface O₃ in YRD. Regionally, the largest surface O₃ reduction of -7.0 ppb is found in central Zhejiang province. However, an increase of surface O₃ up to 6.0 ppb is predicted in the south of Jiangsu province when regional anthropogenic emissions are reduced by 50% (figure 3(f)). This is because southern Jiangsu is considered as a VOC-limited regime due to low HCHO/NO₂ ratios (Wang and Liao 2020,

Li et al 2021, Xu et al 2021). The O₃ concentrations in the region would be elevated with the reduced NO_x emissions alone or the same proportional reduction of VOCs and NO_x emissions (Yang et al 2021). Such phenomenon that O₃ increases with the reduction of VOCs and NO_x emissions in YRD is also observed during the 2019 novel coronavirus pandemic, which provides a natural experiment to assess the effects of precursor changes on surface O₃ (Wang et al 2021, Zhu et al 2021).

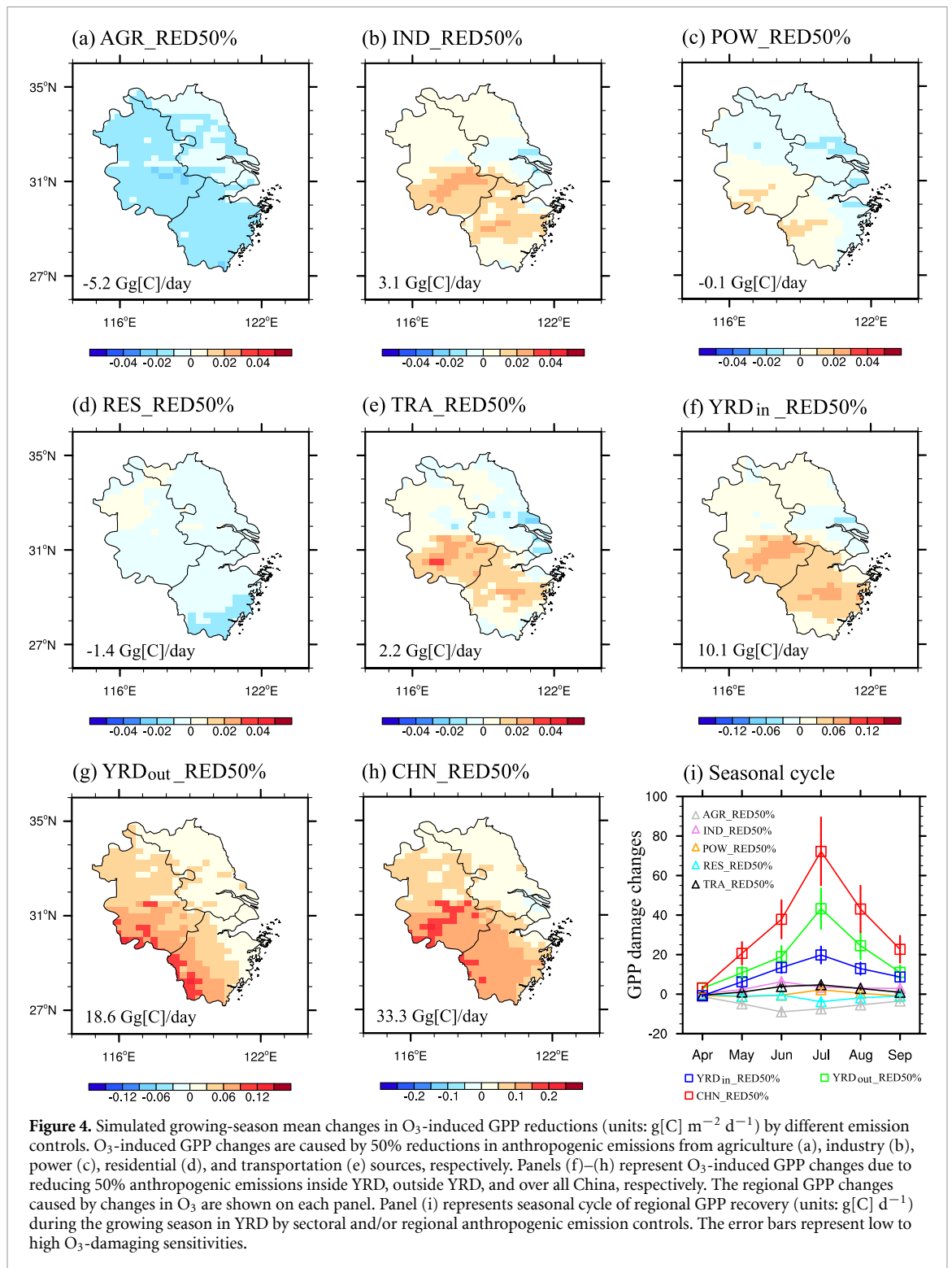


Figure 4. Simulated growing-season mean changes in O_3 -induced GPP reductions (units: $g[C] m^{-2} d^{-1}$) by different emission controls. O_3 -induced GPP changes are caused by 50% reductions in anthropogenic emissions from agriculture (a), industry (b), power (c), residential (d), and transportation (e) sources, respectively. Panels (f)–(h) represent O_3 -induced GPP changes due to reducing 50% anthropogenic emissions inside YRD, outside YRD, and over all China, respectively. The regional GPP changes caused by changes in O_3 are shown on each panel. Panel (i) represents seasonal cycle of regional GPP recovery (units: $g[C] d^{-1}$) during the growing season in YRD by sectoral and/or regional anthropogenic emission controls. The error bars represent low to high O_3 -damaging sensitivities.

Similar to local emission control, the 50% reductions of anthropogenic emissions outside YRD results in a reduction of -1.9 ppb in regional mean O_3 concentrations (figure 3(g)). Such change is most significant in the western YRD with O_3 reductions exceeding -5.0 ppb. The magnitude of O_3 reduction decreases gradually from the west to east, suggesting that regional transport of O_3 and its precursors to YRD is mainly from inland areas. As a comparison, reducing 50% anthropogenic emissions over China

results in a considerable reduction of -4.7 ppb in regional mean surface O_3 over YRD (figure 3(h)), with a spatial pattern merging the O_3 changes by 50% reductions of emissions inside (figure 3(f)) and outside (figure 3(g)) YRD.

We further investigate the seasonal variations in O_3 changes by different anthropogenic emission controls during the growing season in YRD (figure 3(i)). The results show that O_3 reductions driven by regional anthropogenic emission controls,

including YRD_{out}_RED50%, YRD_{in}_RED50%, and CHN_RED50% exhibit similar seasonal variations, increasing from April to July and then decreasing. However, there are inconsistent seasonal variations of O₃ changes driven by sectoral anthropogenic emission controls. The O₃ changes reach a maximum in July for 50% anthropogenic emission reductions in power, transportation, and residential sectors, but in June for 50% anthropogenic emission reductions in agriculture and industry.

3.4. Mitigation of O₃ damages to ecosystem productivity

Emission controls bring benefits to the recovery of ecosystem productivity during the growing season in YRD (figure 4). O₃-induced regional Δ GPP is mitigated by 3.1 ± 0.4 Gg[C] d⁻¹ with 50% emission reductions from industry sector (figure 4(b)) and 2.2 ± 0.2 Gg[C] d⁻¹ with 50% emission reductions from transportation sector (figure 4(e)). However, 50% emission reductions from agriculture, power, and residential sectors result in additional carbon losses of 5.2 ± 0.9 , 0.1 ± 0.1 , and 1.4 ± 0.3 Gg[C] d⁻¹, respectively (figures 4(a), (c) and (d)) due to enhanced regional surface O₃. The sum of regional Δ GPP is -1.5 ± 0.8 Gg[C] d⁻¹ from the individual emission controls at the five sectors during the growing season in YRD.

We further explore the impacts of regional and sectoral collaborative emission controls on ecosystem productivity during the growing season in YRD. With the YRD_{in}_RED50% simulation, the O₃-induced regional Δ GPP is mitigated by 10.1 ± 1.6 Gg[C] d⁻¹ (figure 4(f)), which is much larger than sum of independent emission reduction in five sectors. Such difference illustrates that collaborative emission reductions in all sectors have larger benefits for the recovery of ecosystem productivity. Although there is smaller surface O₃ reduction from YRD_{out}_RED50% than YRD_{in}_RED50% simulations, a larger regional GPP recovery of 18.6 ± 3.5 Gg[C] d⁻¹ is achieved in the former experiment (figure 4(f)). This is because surface O₃ reductions from YRD_{out}_RED50% simulation is mainly located in southwestern YRD (figure 3(f)), where the largest GPP is predicted (figure 1(e)). The largest benefit of ecosystem productivity is simulated by reducing 50% anthropogenic emissions in China, which mitigates O₃-induced Δ GPP by 33.3 ± 6.1 Gg[C] d⁻¹ in YRD (figure 4(h)).

The seasonal variations in GPP recovery from sectoral and regional anthropogenic emission controls follow those in O₃ changes (figure 4(i)). For regional anthropogenic emission controls, the O₃-induced GPP losses are mitigated by 43.2 ± 7.2 , 19.8 ± 3.1 , and 72.2 ± 12.1 Gg[C] d⁻¹ in July for YRD_{out}_RED50%, YRD_{in}_RED50%, and CHN_RED50% simulations,

respectively. These numbers account for 39%, 33%, and 36% of total GPP recovery during the growing season in YRD. For sectoral anthropogenic emission controls, the maximum GPP recovery of 6.3 ± 0.8 Gg[C] d⁻¹ occurs in June for IND_RED50% simulation, but 4.7 ± 0.5 Gg[C] d⁻¹ in July for TRA_RED50% simulation. These results indicate that summer months, especially July are the best period for GPP recovery from anthropogenic emission controls.

4. Conclusion and discussion

The land ecosystems of China are undermined by severe O₃ pollution in recent years. In this study, we combined GEOS-Chem and YIBs models to assess the benefits to ecosystem productivities from sectoral and regional emission controls during the growing season in YRD. For sectoral emission controls, industry and transportation have larger contributions to the recovery of O₃-induced GPP damages than power and residential sectors. Reducing 50% emissions from industry and transportation sectors decrease regional mean surface O₃ by 0.6 and 0.4 ppbv, which can mitigate O₃-induced GPP losses of 3.1 ± 0.4 and 2.2 ± 0.2 Gg[C] d⁻¹ during the growing season in YRD, respectively. For regional pollution controls, the reduction of 50% anthropogenic emissions outside YRD can mitigate a GPP loss of 18.6 ± 3.5 Gg[C] d⁻¹ during the growing season in YRD, which is higher than the 10.1 ± 1.6 Gg[C] d⁻¹ mitigated by a reduction of 50% in local anthropogenic emissions alone. In addition, anthropogenic emission controls in summer months, especially July can bring larger benefits of GPP recovery than the rest period of the growing season.

The predicted O₃ reductions in YRD by shutting down all anthropogenic emission in China are comparable to previous studies (Wang *et al* 2011, Lu *et al* 2019). Our simulated GPP recoveries from independent sectoral emission controls are in general consistent with simulations by Unger *et al* (2020), except that the latter predicted a positive contribution by agriculture emission reductions to mitigating O₃-induced carbon losses while we predicted an opposite contribution with negative effects. In the GAINS inventory used in Unger *et al* (2020), agriculture sector includes NO_x, CH₄ and NH₃ gases, which affect O₃ production substantially. However, the agriculture sector in the MEIC inventory used in this study includes only NH₃, leading to increases of surface O₃ following the decreased ammonium and PM_{2.5}. In addition, compared with global assessment by Unger *et al* (2020), our regional assessment reveals some new insights for the benefits of GPP recovery from anthropogenic emission controls: (a) the responses of GPP recovery show large spatial heterogeneity. The 50% reduction

of emissions from industry and transportation sectors results in a general recovery of O₃-induced GPP reductions in YRD, but with regional degradation in eastern Jiangsu province, which is defined as a VOC-limited regime. (b) Compared to emission controls of a single sector, collaborative emission reductions in all sectors have larger benefits for the recovery of O₃-induced GPP losses. With 50% emission reductions in all sectors in YRD, the O₃-induced regional ΔGPP is mitigated by 10.1 ± 1.6 Gg[C] d⁻¹, which is much larger than sum of independent emission reduction in five sectors. (c) Anthropogenic emission control outside the region is also an effective way to mitigate local O₃-induced GPP losses. The GPP recovery by a 50% emission cut outside YRD is about twice that by a 50% emission cut inside YRD. This is because the regional GPP recovery is dependent on both O₃ changes and the forest coverage. (d) The efficiencies of anthropogenic emission controls on GPP recovery vary through the growing season. Summer, especially July is the best period for recovery of O₃-induced GPP losses by anthropogenic emission controls. (e) The net effect of emission control on GPP recovery is nonlinear. The 50% reduction of all emissions results in a GPP recovery of 33.3 ± 6.1 Gg[C] d⁻¹ in YRD, accounting for only 18% of the total regional GPP losses (figure 2(a)). As a comparison, the 100% reduction of all anthropogenic emissions leads to a GPP recovery of 144.9 ± 31.5 Gg[C] d⁻¹, which is up to 79% of the total GPP loss. Such nonlinearity suggests that only the deep cut of anthropogenic emissions (e.g. >50%) can bring effective benefits to the ecosystem carbon assimilation.

Our study revealed large benefits of recovering ecosystem functions associated with the pollution reduction towards carbon neutrality. Currently, reductions of emissions from industry and transportation sectors brings the largest benefits to the recovery of carbon uptake by land ecosystems in YRD. Such benefits will be much stronger with simultaneous emission controls of multiple sectors and regions than a single sector or from local areas. These gains in carbon sequestration, though likely vary from cities to metropolitans, should be considered to in part offset the large costs in the air pollution regulation. In our current estimate, we applied a constant 50% reduction rate for all emission sectors. However, the cost of emission control varies among sectors and regions, leading to varied reduction percentages for O₃ precursors in reality. Therefore, scientific pathways of emission reduction are required and the associated GPP recovery need further investigations.

Data availability statement

The data that support the findings of this study are available upon reasonable request from the authors.

Acknowledgments


This work was supported by the Jiangsu Science Fund for Distinguished Young Scholars (Grant No. BK20200040).

Conflict of interest

The authors declare no competing interests.

ORCID iDs

Xu Yue  <https://orcid.org/0000-0002-8861-8192>

Zhili Wang  <https://orcid.org/0000-0002-4392-3230>

Lin Zhang  <https://orcid.org/0000-0003-2383-8431>

References

- Agathokleous E *et al* 2020 Ozone affects plant, insect, and soil microbial communities: a threat to terrestrial ecosystems and biodiversity *Sci. Adv.* **6** eabc1176
- Atkinson R 2000 Atmospheric chemistry of VOCs and NO_x *Atmos. Environ.* **34** 2063–101
- Bian H S and Prather M J 2002 Fast-J2: accurate simulation of stratospheric photolysis in global chemical models *J. Atmos. Chem.* **41** 281–96
- Chen C, Zhao B and Weschler C J 2012 Assessing the influence of indoor exposure to ‘outdoor ozone’ on the relationship between ozone and short-term mortality in US communities *Environ. Health Perspect.* **120** 235–40
- Chen S and Brune W H 2012 Global sensitivity analysis of ozone production and O₃-NO_x-VOC limitation based on field data *Atmos. Environ.* **55** 288–96
- Clark D B *et al* 2011 The Joint UK Land Environment Simulator (JULES), model description—part 2: carbon fluxes and vegetation dynamics *Geosci. Model. Dev.* **4** 701–22
- Dang R J, Liao H and Fu Y 2021 Quantifying the anthropogenic and meteorological influences on summertime surface ozone in China over 2012–2017 *Sci. Total Environ.* **754** 142394
- Fang J Y, Yu G R, Liu L L, Hu S J and Chapin F S 2018 Climate change, human impacts, and carbon sequestration in China introduction *Proc. Natl Acad. Sci. USA* **115** 4015–20
- Farquhar G D, Caemmerer S V and Berry J A 1980 A biochemical model of photosynthetic CO₂ assimilation in leaves of C₃ species *Planta* **149** 78–90
- Feng Z Z, Hu E Z, Wang X K, Jiang L J and Liu X J 2015 Ground-level O₃ pollution and its impacts on food crops in China: a review *Environ. Pollut.* **199** 42–48
- Friedlingstein P *et al* 2020 Global carbon budget 2020 *Earth Syst. Sci. Data* **12** 3269–340
- Fu Y, Liao H and Yang Y 2019 Interannual and decadal changes in tropospheric ozone in China and the associated chemistry-climate interactions: a review *Adv. Atmos. Sci.* **36** 975–93
- Gong C and Liao H 2019 A typical weather pattern for ozone pollution events in North China *Atmos. Chem. Phys.* **19** 13725–40
- Gong C, Liao H, Yue X, Ma Y M and Lei Y D 2021 Impacts of ozone-vegetation interactions on ozone pollution episodes in North China and the Yangtze River Delta *Geophys. Res. Lett.* **48** e2021GL093814
- Guenther A B, Jiang X, Heald C L, Sakulyanontvittaya T, Duhl T, Emmons L K and Wang X 2012 The Model of Emissions of Gases and Aerosols from Nature version 2.1 (MEGAN2.1): an extended and updated framework for modeling biogenic emissions *Geosci. Model. Dev.* **5** 1471–92

- He J *et al* 2022 Towards carbon neutrality: a study on China's long-term low-carbon transition pathways and strategies *Environ. Sci. Ecotechnol.* **9** 100134
- He Q Q, Zhang M, Song Y M and Huang B 2021 Spatiotemporal assessment of PM_{2.5} concentrations and exposure in China from 2013 to 2017 using satellite-derived data *J. Clean. Prod.* **286** 124965
- Hoesly R M *et al* 2018 Historical (1750–2014) anthropogenic emissions of reactive gases and aerosols from the Community Emissions Data System (CEDS) *Geosci. Model. Dev.* **11** 369–408
- Jiang W X, Wang L C, Zhang M, Yao R, Chen X X, Gui X, Sun J and Cao Q 2021 Analysis of drought events and their impacts on vegetation productivity based on the integrated surface drought index in the Hanjiang River Basin, China *Atmos. Res.* **254** 105536
- Kim P S *et al* 2015a Sources, seasonality, and trends of southeast US aerosol: an integrated analysis of surface, aircraft, and satellite observations with the GEOS-Chem chemical transport model *Atmos. Chem. Phys.* **15** 10411–33
- Kim Y, Moorcroft P R, Aleinov I, Puma M J and Kiang N Y 2015b Variability of phenology and fluxes of water and carbon with observed and simulated soil moisture in the Ent Terrestrial Biosphere Model (Ent TBM version 1.0.1.0.0) *Geosci. Model. Dev.* **8** 3837–65
- Lamboll R D, Jones C D, Skeie R B, Fiedler S, Samset B H, Gillett N P, Rogelj J and Forster P M 2021 Modifying emissions scenario projections to account for the effects of COVID-19: protocol for CovidMIP *Geosci. Model. Dev.* **14** 3683–95
- Lee H M, Park R J, Henze D K, Lee S, Shim C, Shin H J, Moon K J and Woo J H 2017 PM_{2.5} source attribution for Seoul in May from 2009 to 2013 using GEOS-Chem and its adjoint model *Environ. Pollut.* **221** 377–84
- Lei Y D *et al* 2021 Indirect contributions of global fires to surface ozone through ozone-vegetation feedback *Atmos. Chem. Phys.* **21** 11531–43
- Lei Y D, Yue X, Liao H, Gong C and Zhang L 2020 Implementation of Yale Interactive terrestrial Biosphere model v1.0 into GEOS-Chem v12.0.0: a tool for biosphere-chemistry interactions *Geosci. Model. Dev.* **13** 1137–53
- Lei Y *et al* 2022 Global perspective of drought impacts on ozone pollution episodes *Environ. Sci. Technol.* **56** 3932–40
- Li K, Jacob D J, Liao H, Zhu J, Shah V, Shen L, Bates K H, Zhang Q and Zhai S X 2019 A two-pollutant strategy for improving ozone and particulate air quality in China *Nat. Geosci.* **12** 906
- Li K, Jacob D J, Shen L, Lu X, de Smedt I and Liao H 2020 Increases in surface ozone pollution in China from 2013 to 2019: anthropogenic and meteorological influences *Atmos. Chem. Phys.* **20** 11423–33
- Li L *et al* 2021 Modelling air quality during the EXPLORE-YRD campaign—part II. Regional source apportionment of ozone and PM_{2.5} *Atmos. Environ.* **247** 118063
- Lin M Y, Horowitz L W, Xie Y Y, Paulot F, Malyshev S, Shevliakova E, Finco A, Gerosa G, Kubistin D and Pilegaard K 2020 Vegetation feedbacks during drought exacerbate ozone air pollution extremes in Europe *Nat. Clim. Change* **10** 444
- Liu Y M and Wang T 2020 Worsening urban ozone pollution in China from 2013 to 2017—part I: the complex and varying roles of meteorology *Atmos. Chem. Phys.* **20** 6305–21
- Lombardozzi D, Levis S, Bonan G, Hess P G and Sparks J P 2015 The influence of chronic ozone exposure on global carbon and water cycles *J. Clim.* **28** 292–305
- Lu X, Zhang L, Chen Y F, Zhou M, Zheng B, Li K, Liu Y M, Lin J T, Fu T-M and Zhang Q 2019 Exploring 2016–2017 surface ozone pollution over China: source contributions and meteorological influences *Atmos. Chem. Phys.* **19** 8339–61
- Lu X, Zhang L, Wang X L, Gao M, Li K, Zhang Y Z, Yue X and Zhang Y H 2020 Rapid increases in warm-season surface ozone and resulting health impact in China since 2013 *Environ. Sci. Technol. Lett.* **7** 240–7
- Ma X D, Huang J P, Zhao T L, Liu C, Zhao K H, Xing J and Xiao W 2021 Rapid increase in summer surface ozone over the North China Plain during 2013–2019: a side effect of particulate matter reduction control? *Atmos. Chem. Phys.* **21** 1–16
- Piao S L, Fang J Y, Ciais P, Peylin P, Huang Y, Sitch S and Wang T 2009 The carbon balance of terrestrial ecosystems in China *Nature* **458** 1009–U82
- Porter W C and Heald C L 2019 The mechanisms and meteorological drivers of the summertime ozone-temperature relationship *Atmos. Chem. Phys.* **19** 13367–81
- Qu Y W, Voulgarakis A, Wang T J, Kasoar M, Wells C, Yuan C, Varma S and Mansfield L 2021 A study of the effect of aerosols on surface ozone through meteorology feedbacks over China *Atmos. Chem. Phys.* **21** 5705–18
- Sitch S, Cox P M, Collins W J and Huntingford C 2007 Indirect radiative forcing of climate change through ozone effects on the land-carbon sink *Nature* **448** 791–U4
- Spitters C 1986 Separating the diffuse and direct component of global radiation and its implications for modeling canopy photosynthesis part II—calculation of canopy photosynthesis *Agric. For. Meteorol.* **38** 231–42
- Tong D *et al* 2020 Dynamic projection of anthropogenic emissions in China: methodology and 2015–2050 emission pathways under a range of socio-economic, climate policy, and pollution control scenarios *Atmos. Chem. Phys.* **20** 5729–57
- Unger N, Zheng Y Q, Yue X and Harper K L 2020 Mitigation of ozone damage to the world's land ecosystems by source sector *Nat. Clim. Change* **10** 134–7
- Wan W X, Manning W J, Wang X K, Zhang H X, Sun X and Zhang Q Q 2014 Ozone and ozone injury on plants in and around Beijing, China *Environ. Pollut.* **191** 215–22
- Wang Y and Liao H 2020 Effect of emission control measures on ozone concentrations in Hangzhou during G20 meeting in 2016 *Chemosphere* **261** 127729
- Wang Y, Zhang Y, Hao J and Luo M 2011 Seasonal and spatial variability of surface ozone over China: contributions from background and domestic pollution *Atmos. Chem. Phys.* **11** 3511–25
- Wang Y, Zhu S Q, Ma J L, Shen J Y, Wang P F, Wang P and Zhang H L 2021 Enhanced atmospheric oxidation capacity and associated ozone increases during COVID-19 lockdown in the Yangtze River Delta *Sci. Total Environ.* **768** 144796
- Wesely M L 1989 Parameterization of surface resistances to gaseous dry deposition in regional-scale numerical-models *Atmos. Environ.* **23** 1293–304
- Xu J W, Huang X, Wang N, Li Y Y and Ding A J 2021 Understanding ozone pollution in the Yangtze River Delta of eastern China from the perspective of diurnal cycles *Sci. Total Environ.* **752** 141928
- Yang Y, Zhao Y, Zhang L, Zhang J, Huang X, Zhao X F, Zhang Y, Xi M X and Lu Y 2021 Improvement of the satellite-derived NO_x emissions on air quality modeling and its effect on ozone and secondary inorganic aerosol formation in the Yangtze River Delta, China *Atmos. Chem. Phys.* **21** 1191–209
- Yu T, Sun R, Xiao Z Q, Zhang Q, Liu G, Cui T X and Wang J M 2018 Estimation of global vegetation productivity from Global Land Surface Satellite data *Remote Sens.* **10** 327
- Yuan W P *et al* 2010 Global estimates of evapotranspiration and gross primary production based on MODIS and global meteorology data *Remote Sens. Environ.* **114** 1416–31
- Yue X and Unger N 2015 The Yale Interactive terrestrial Biosphere model version 1.0: description, evaluation and implementation into NASA GISS ModelE2 *Geosci. Model. Dev.* **8** 2399–417
- Yue X and Unger N 2018 Fire air pollution reduces global terrestrial productivity *Nat. Commun.* **9** 5413

- Yue X, Unger N, Harper K, Xia X G, Liao H, Zhu T, Xiao J F, Feng Z Z and Li J 2017 Ozone and haze pollution weakens net primary productivity in China *Atmos. Chem. Phys.* **17** 6073–89
- Yue X, Unger N and Zheng Y 2015 Distinguishing the drivers of trends in land carbon fluxes and plant volatile emissions over the past 3 decades *Atmos. Chem. Phys.* **15** 11931–48
- Zhang Q et al 2019 Drivers of improved PM_{2.5} air quality in China from 2013 to 2017 *Proc. Natl Acad. Sci. USA* **116** 24463–9
- Zhao K H et al 2022 Understanding the underlying mechanisms governing the linkage between atmospheric oxidative capacity and ozone precursor sensitivity in the Yangtze River Delta, China: a multi-tool ensemble analysis *Environ. Int.* **160** 107060
- Zhao X et al 2013 The Global Land Surface Satellite (GLASS) remote sensing data processing system and products *Remote Sens.* **5** 2436–50
- Zheng B et al 2018 Trends in China's anthropogenic emissions since 2010 as the consequence of clean air actions *Atmos. Chem. Phys.* **18** 14095–111
- Zhou S S, Tai A P K, Sun S H, Sadiq M, Heald C L and Geddes J A 2018 Coupling between surface ozone and leaf area index in a chemical transport model: strength of feedback and implications for ozone air quality and vegetation health *Atmos. Chem. Phys.* **18** 14133–48
- Zhu S Q, Poetscher J, Shen J Y, Wang S Y, Wang P and Zhang H L 2021 Comprehensive insights into O₃ changes during the COVID-19 from O₃ formation regime and atmospheric oxidation capacity *Geophys. Res. Lett.* **48** e2021GL093668